Check for updates

New Phytologist

Research

High photosynthesis rates in *Brassiceae* species are mediated by leaf anatomy enabling high biochemical capacity, rapid CO_2 diffusion and efficient light use

Moges A. Retta[1], Leen Van Doorselaer[2], Steven M. Driever[1], Xinyou Yin[1], Norbert C. A. de Ruijter[3], Pieter Verboven[2], Bart M. Nicolaï[2] and Paul C. Struik[1]

[1]Centre for Crop Systems Analysis, Wageningen University & Research, PO Box 430, 6700 AK, Wageningen, the Netherlands; [2]Mechatronics, Biostatistics and Sensors (MeBioS), Biosystems Department, KU Leuven, Willem de Croylaan 42, B-3001, Leuven, Belgium; [3]Laboratory of Cell and Developmental Biology, Wageningen Light Microscopy Centre (WLMC), Wageningen University & Research, PO Box 633, 6700 AP, Wageningen, the Netherlands

Author for correspondence:
Paul C. Struik
Email: paul.struik@wur.nl

Received: *14 May 2024*
Accepted: *31 August 2024*

New Phytologist (2024)
doi: 10.1111/nph.20136

Key words: 3D leaf anatomy, Chl content profile, *Hirschfeldia incana*, light absorbance profile, mesophyll conductance, photosynthesis.

Summary

- Certain species in the *Brassicaceae* family exhibit high photosynthesis rates, potentially providing a valuable route toward improving agricultural productivity. However, factors contributing to their high photosynthesis rates are still unknown.
- We compared *Hirschfeldia incana*, *Brassica nigra*, *Brassica rapa* and *Arabidopsis thaliana*, grown under two contrasting light intensities.
- *Hirschfeldia incana* matched *B. nigra* and *B. rapa* in achieving very high photosynthesis rates under high growth-light condition, outperforming *A. thaliana*. Photosynthesis was relatively more limited by maximum photosynthesis capacity in *H. incana* and *B. rapa* and by mesophyll conductance in *A. thaliana* and *B. nigra*. Leaf traits such as greater exposed mesophyll specific surface enabled by thicker leaf or high-density small palisade cells contributed to the variation in mesophyll conductance among the species. The species exhibited contrasting leaf construction strategies and acclimation responses to low light intensity. High-light plants distributed Chl deeper in leaf tissue, ensuring even distribution of photosynthesis capacity, unlike low-light plants.
- Leaf anatomy of *H. incana*, *B. nigra* and *B. rapa* facilitated effective CO_2 diffusion, efficient light use and provided ample volume for their high maximum photosynthetic capacity, indicating that a combination of adaptations is required to increase CO_2-assimilation rates in plants.

Introduction

Enhancing photosynthesis is vital for averting food shortages by boosting crop yields (Zhu *et al.*, 2010; Ort *et al.*, 2015; Simkin *et al.*, 2019). Exploring the photosynthesis of wild relatives of cultivated crops may reveal novel genetic and physiological factors contributing to high photosynthetic rates (Adachi *et al.*, 2013; Taylor *et al.*, 2020; Mathan *et al.*, 2021). Agriculturally important crops from the mustard family, such as *Brassica nigra* and *Brassica oleracea*, have recently been observed to exhibit high photosynthesis rates under high light, which have been linked to their high biochemical capacity (Taylor *et al.*, 2020). Their wild relative *Hirschfeldia incana* exhibited even higher photosynthesis rates at high light intensity (Garassino *et al.*, 2022). *Brassica nigra* and *Brassica rapa* are economically important crop species, and genetically close to other important crops, and could thus be a valuable resource for increasing photosynthesis in cultivated crops (Taylor *et al.*, 2022). However, the anatomical, biochemical and physiological bases of the relatively high photosynthetic competence of these species are yet to be revealed.

Photosynthesis in the *Brassicaceae* family like in other plants can be limited by multiple factors (Taylor *et al.*, 2020, 2022; Schlüter *et al.*, 2023). It is limited by stomatal conductance (g_s), which is the conductance of the diffusion of CO_2 from the ambient air into the stomatal cavity. Subsequent CO_2 diffusion to fixation sites encounters gas- and liquid-phase resistances, collectively termed mesophyll resistance or the inverse mesophyll conductance (g_m). g_m is another important limitation to photosynthesis, influenced by the physical properties of the intercellular airspace, cell wall and chloroplasts (Earles *et al.*, 2018; Théroux-Rancourt *et al.*, 2023). Both photosynthesis and g_m scale with the exposed chloroplast surface per leaf area (S_c) and the exposed mesophyll surface area (S_m) per leaf area ($S_{m,a}$) (Terashima *et al.*, 2001; Ren *et al.*, 2019; Lundgren & Fleming, 2020; Evans, 2021; Knauer *et al.*, 2022; Zeng *et al.*, 2022; Xiong, 2023). Recent advancements emphasize the need for a 3D assessment of mesophyll structural traits to better

© 2024 The Author(s).
New Phytologist © 2024 New Phytologist Foundation.
This is an open access article under the terms of the Creative Commons Attribution License, which permits use, distribution and reproduction in any medium, provided the original work is properly cited.

understand their role in photosynthesis (Berghuijs *et al.*, 2015; Mathers *et al.*, 2018; Earles *et al.*, 2019; Ren *et al.*, 2019; Harwood *et al.*, 2020; Théroux-Rancourt *et al.*, 2021, 2023). Additionally, mesophyll structure impacts the distribution of light in leaves via altered intra-leaf profiles of Chl abundance and light absorption influencing photosynthesis rates across different species (Cui *et al.*, 1991; Tholen *et al.*, 2012; Slattery *et al.*, 2016; Borsuk & Brodersen, 2019; Poorter *et al.*, 2019). While the columnar palisade tissue enhances light penetration into the mesophyll, spongy tissue enhance light absorption by scattering light (Terashima *et al.*, 2011; Ichiro *et al.*, 2016). Furthermore, photosynthesis faces limitations, primarily by factors such as the maximum rate of carboxylation (V_{cmax}) of the enzyme Rubisco (ribulose-1,5-bisphosphate carboxylase/oxygenase) (Farquhar *et al.*, 1980; von Caemmerer & Farquhar, 1981; Evans, 2013) and the maximum rate of linear electron transport (J_{max}) (Evans, 2013; Yamori *et al.*, 2016). Understanding the multifaceted constraints imposed by leaf traits holds promise for enhancing photosynthetic efficiency (Evans, 2013; Mathan *et al.*, 2021).

Enhancing the adaptation of photosynthesis to diverse environmental settings is required to increase yield (Simkin *et al.*, 2019). Light availability is one of the most important environmental factors constraining plant productivity (Boardman, 1977). Recent investigation of 3D mesophyll structure in relation to intra-leaf profiles of light absorption and Chl content at high resolution shed new lights on acclimation responses to water and light availability (Slattery *et al.*, 2016; Borsuk & Brodersen, 2019; Lundgren & Fleming, 2020; Anderson *et al.*, 2021; Momayyezi *et al.*, 2022; Théroux-Rancourt *et al.*, 2023). While the leaf physiological, morphological and anatomical responses to changes in growth light intensity are well-established, prime leaf traits contributing to the acclimation responses optimizing photosynthesis depends on the species (Boardman, 1977; Terashima *et al.*, 2001; Hoshino *et al.*, 2019; Poorter *et al.*, 2019).

This study aimed to examine the relatively high photosynthetic performance of three genetically closely related species – *H. incana*, *B. nigra* and *B. rapa* – in relation to leaf anatomy (Arias & Pires, 2012). We characterized their photosynthesis rate, CO_2 conductance, 3D leaf anatomy and the intra-leaf Chl and light profiles, in comparison with the model species *Arabidopsis thaliana*. By growing the plants under both low and high light intensities, we aim to examine how the acclimation responses influence their photosynthetic performance. It was shown previously that the three *Brassiceae* exceeded *A. thaliana* in photosynthesis rate at high light intensity (Garassino *et al.*, 2022). We hypothesize that the higher photosynthesis rate at high light intensity of *H. incana*, *B. nigra* and *B. rapa* is facilitated by greater CO_2 transport efficiency and effective light use mediated by mesophyll structure. We expect that these species will exhibit coordinated changes in their mesophyll structure and maximum photosynthesis capacity in response to low-light conditions to allow for a higher photosynthesis rate than in *A. thaliana*.

Materials and Methods

Plant material and growth conditions

Hirschfeldia incana L. (7^{th}-generation inbred line 190 003 HIN-NIJ-07-B from an accession collected in Nijmegen, the Netherlands), *Brassica nigra* L. (3rd-generation inbred line 210 093 BNI-DG1-03-B, from an accession collected in Wageningen, the Netherlands), *Brassica rapa* L. (inbred line 'R-o-18') and *Arabidopsis thaliana* (accession Columbia) were grown on rock-wool blocks (Grodan Plantop, Roermond, the Netherlands, 10 × 10 × 7.5 cm) and fertigated with a nitrogen-rich nutrient solution (1.2 mM $NH4^+$, 7.2 mM K^+, 4 mM Ca^{2+}, 1.82 mM Mg^{2+}, 12.4 mM NO_3, 3.32 mM SO_4^{2-}, 1 mM P, 35 µM Fe^{3+}, 8 µM Mn^{2+}, 5 µm Zn^{2+}, 20 µM B, 0.5 µM Cu^{2+}, 0.5 µM Mo^{4+}) using an automated dripping system. The plants were grown under a light intensity of 200 µmol m^{-2} s^{-1} (with 11.7% spatial variation) and 1800 µmol m^{-2} s^{-1} (12.0% spatial variation) achieved with high-output LED light modules (Fluence VYPR2p, PhysioSpec™ Indoor spectrum, USA). Growth conditions were 12 h : 12 h, day : night, relative humidity of 70% and day : night temperatures of 23°C : 20°C, respectively.

Leaf gas exchange and Chl fluorescence measurements

The net photosynthesis (A_n) responses to incident irradiance (I_{inc}) and intercellular CO_2 concentration (C_i) were measured in four replicates by enclosing the mid-position of the youngest fully expanded leaf from a plant on the 28th day after sowing using a LI-6800 (Li-Cor, Lincoln, NE, USA). Initially, the leaves underwent a 20-min dark adaptation. The A_n/I_{inc} curve was assessed at increasing I_{inc} values of 75, 100, 125, 150, 175, 200, 300, 400, 550, 800, 1100, 1500, 1800, 2200 µmol m^{-2} s^{-1} at 21% O_2 and 400 µmol mol^{-1} CO_2 and at I_{inc} values up to 400 µmol m^{-2} s^{-1} at 2% O_2 and 1000 µmol mol^{-1} CO_2. The A_n/C_i curve was measured by using the external CO_2 concentrations (C_a) values of 400, 300, 250, 200, 150, 100, 400, 400, 500, 600, 700, 850, 1000, 1200, 1500 µmol mol^{-1} at 21% O_2 and 2200 µmol m^{-2} s^{-1} I_{inc}. The adaptation time between the steps was 6 min. A leaf temperature of 25°C was maintained, along with a leaf-to-air vapor pressure difference of 1.0–1.6 kPa. The quantum yield of PSII (Φ_2) was calculated from measurements of the maximum fluorescence in light using multiphase flash (> 8000 µmol m^{-2} s^{-1}) and steady-state fluorescence (Genty *et al.*, 1989; Loriaux *et al.*, 2013). Gas exchange data for *A. thaliana* were corrected for the actual leaf area within the 2 cm^2 cuvette of the LI-6800 by measuring the area from photographs using ImageJ (National Institutes of Health, Bethesda, MD, USA).

Leaf dry mass and nitrogen content

Two leaf samples of 2 cm^2 area from each replicate plant from the area and the whole leaf blade of known area for *A. thaliana* were then dried at 70°C to a constant dry weight to calculate leaf

© 2024 The Author(s).
New Phytologist © 2024 New Phytologist Foundation.

14698137, 0, Downloaded from https://nph.onlinelibrary.wiley.com/doi/10.1111/nph.20136 by Wageningen University And Research Facilitair Bedrijf, Wiley Online Library on [21/10/2024]. See the Terms and Conditions (https://onlinelibrary.wiley.com/terms-and-conditions) on Wiley Online Library for rules of use; OA articles are governed by the applicable Creative Commons License

14698137, 0, Downloaded from https://nph.onlinelibrary.wiley.com/doi/10.1111/nph.20136 by Wageningen University And Research Facilitair Bedrijf, Wiley Online Library on [21/10/2024]. See the Terms and Conditions (https://onlinelibrary.wiley.com/terms-and-conditions) on Wiley Online Library for rules of use; OA articles are governed by the applicable Creative Commons License

mass per area. The nitrogen concentration was analyzed using an element analyzer based on the micro-Dumas combustion method. The leaf nitrogen content per leaf area was then calculated from the nitrogen concentration and leaf dry mass per area.

Chlorophyll content profile

Measurement of optical properties A leaf disk of 1 cm diameter punched out from the area nearby the gas exchange measurement was measured for leaf transmittance and reflectance using a dual channel spectrophotometer and a double integrating sphere set up (Wassenaar *et al.*, 2022) using a spectrum of wavelength of 450–700 nm applied on the top leaf surface.

Leaf Chl content and mesophyll Chl profiles Profiles of Chl content were assessed based on reported methods (Vogelmann & Evans, 2002; Slattery *et al.*, 2016; Borsuk & Brodersen, 2019). A separate set of plants were grown under the same conditions as those used for gas exchange measurements. Uniform leaf age and sampling locations were maintained, with 20-min dark adaptation preceding measurements. Three leaves per species per treatment were sampled from three different plants.

To analyze the Chl profile, 200 ± 10-μm-thick sections were made from a sample (0.5 cm × 1.5 cm) using a sliding microtome (Leica, Germany), and they were incubated in water under low pressure (0.1–0.2 bar) to fill intercellular cavities. Four sections were imaged per leaf sample per plant using Leica DM8 inverted scope equipped with a Stellaris 5 confocal microscope (Leica Microsystems, Wetzlar, Germany). The sections were scanned with a 490 nm excitation laser line (at 7% intensity of an 85% intensity white light laser) and Chl autofluorescence was recorded in a spectral range of 660–700 nm with Leica objective ×10/0.4 NA (optical slice thickness of 7.12 μm, pixel size of 2.275 × 2.275 μm at 1.0 zoom). *Z*-stacks were made with an accurate galvo-z-stage over 85–112 μm depth (avoiding the cut faces), comprising 13–18 nonoverlapping leaf cross sections, at two random positions per sample.

At the end of the measurement, a leaf sample of 1 cm diameter was taken from a nearby area, freeze-dried using liquid nitrogen and stored at −80°C for Chl content analysis. The Chl was extracted using 3 ml of dimethyl-formamide solution per leaf sample. A 1 ml of extract was analyzed using a spectrophotometer (2 nm band-pass resolution). The concentrations of total Chl, Chl*a* and Chl*b* content were calculated according to Wellburn (1994).

To calculate the relative fluorescence, the intensity of pixels having the same pair of *x* and *y* coordinates was summed pixel by pixel in depth along the *z*-direction, starting from the cut face. From the resulting total intensity, the mean intensity of pixels along the direction parallel to the epidermis was calculated, in ImageJ from the upper mesophyll across the leaf thickness to the lower mesophyll, excluding the epidermis. The relative fluorescence was calculated by dividing the mean intensity at each depth by the maximum intensity of each species and treatment. The relative depth was calculated for each section by dividing each depth by the maximum depth, excluding the epidermis. Means and SD of the relative fluorescence of 24–36 sections per species per treatment (two *z*-stacks from three sections per sample and one sample per plant from four plants per treatment) were calculated.

Light and electron microscopy of leaf sections

A leaf sample of 2 cm^2 area for each plant was put immediately in a fixative solution made of 2.5% glutaraldehyde and 2% paraformaldehyde in 0.1 M phosphate/citrate buffer and kept at 4°C before fixation in cold 2% glutaraldehyde, buffered at pH 7.3 with 50 mM Na-cacodylate and 150 mM saccharose. Afterwards, the samples were dehydrated using a graded acetone series, embedded in Araldite® and sectioned with a Leica EM UC6 ultra-microtome (Leica Microsystems GmbH, Wetzlar, Germany). Postfixation was then carried out using 2% osmium tetroxide in the same buffer. Double-stained 70 nm thin sections were examined in a Zeiss EM900 electron microscope (Zeiss, Oberkochen, Germany).

The mesophyll cells were imaged at ×400 and ×700, depending on the cell size across species, to measure the fraction of exposed mesophyll surface covered by chloroplasts as the ratio of the length of the exposed chloroplast and length of exposed mesophyll surface. The cell wall was imaged at ×20 000 and the chloroplasts were imaged at ×3000 to measure their thickness.

X-ray micro-CT imaging of leaf anatomy

The same set of plants used for light-sheet microscopy was used for imaging alongside additional plants grown in the same conditions, maintaining consistent leaf age and sampling location. A sample of 2 mm × 5 mm was enclosed between two pieces of Kapton tape and secured in a pipette tip for mounting in the sample holder. X-ray projection images of the leaf sample were obtained using a UniTom HR micro-CT system (Tescan XRE NV, Ghent, Belgium) at 75 kV and 1 W. 1900 projections with a voxel resolution of 855 nm were captured per sample. With an exposure time of 1100 ms, this resulted in a total scan time of 45 min for each leaf tissue sample. The projections were reconstructed using the filtered back-projection method in Panthera (Tescan XRE NV, Ghent, Belgium).

A volume of 0.5 mm × 0.5 mm × leaf thickness was selected and filtered using nonlocal means filtering with spatial standard deviation of 2 in Avizo 2020.3.1 (Thermo Fisher Scientific, Waltham, MA, USA). The steps of the image processing protocol are shown in Supporting Information Fig. S1. Initial segmentation of this volume into mesophyll and epidermis regions was carried out using the procedure of Théroux-Rancourt *et al.* (2020). The vein was manually segmented over multiple 2D slices from the paradermal view using a region growing algorithm and interpolated to retrieve the 3D segmentation in Avizo. The initial segmentations of the epidermis and veins were then manually further refined in transversal view to get the full 3D segmentation.

Leaf anatomical features, such as the mesophyll porosity, mesophyll thickness, the surface area of the exposed mesophyll cell per leaf area ($S_{m,a}$) and per mesophyll volume ($S_{m,v}$), were assessed (Notes S1). The exposed chloroplast surface per leaf area

© 2024 The Author(s).
New Phytologist © 2024 New Phytologist Foundation.

(S_c) was calculated as a product of S_c: $S_{m,a}$, which was assumed as the length ratio measured from light microscope images, and $S_{m,a}$. To measure the diameter of palisade cells and their density (the number of cells per image area), paradermal sections were made at 40% leaf thickness, which was approximately at the middle of the palisade parenchyma. The paradermal slices were then segmented in CELLPOSE 2.0 (Stringer *et al.*, 2021), and the labels touching the borders of the image were removed. Cell density was determined by counting the remaining labels in the 0.25 mm^2 area. The median area of the individual cells ($n > 100$) was used to calculate the diameter of an equivalent disk, serving as a proxy for palisade diameter.

Estimation of maximum photosynthesis capacity parameters and mesophyll conductance

The responses of A_n to C_i and I_{inc} were fitted to a biochemical model of C_3 photosynthesis (Farquhar *et al.*, 1980; Yin *et al.*, 2021) to estimate the maximum Rubisco carboxylation rate (V_{cmax}), the maximum rate of electron transport (J_{max}), the rate of triose-phosphate utilization (T_p) and mesophyll conductance from gas exchange ($g_{m,cf}$) for each replicate plant. The rate of day respiration, R_d, pre-estimated from 2% O_2 measurements using the Yin method (Yin & Amthor, 2024), was an input in the fitting. We assumed the Michaelis–Menten kinetic constant of Rubisco carboxylation, K_{mC} = 267 μbar and that of oxygenation, K_{mO} = 164 mbar. The Rubisco specificity factor $S_{C/O}$ was assumed 2.86 mbar μbar^{-1} at 25°C (von Caemmerer, 2013). We used the irradiance and CO_2 response of photosynthesis measured at 21% O_2 in the curve fitting in SAS (SAS Institute Inc., NC, USA) (Yin *et al.*, 2009). Model equations and more explanations of the fitting are given in Notes S2.

Calculation of light absorbance and photosynthesis across leaf depth

The profiles of light absorbance and photosynthesis across leaf depth were calculated using profiles of Chl content and a multilayer model of leaf photosynthesis (Terashima & Saeki, 1985; Evans, 1995; Slattery *et al.*, 2016). The profile of relative fluorescence was converted into a Chl content profile using the measured Chl content. An apparent extinction coefficient was calculated from total absorbance (see 'Measurement of optical properties' in the Materials and Methods), the total Chl content and mesophyll thickness measured from the confocal images using Beer's law (Slattery *et al.*, 2016). The absorbed light of a leaf layer was calculated using Beer–Lambert's law, and the calculated apparent extinction coefficient, assuming an irradiance of 2200 μmol m^{-2} s^{-1}, was applied on the top leaf surface. The A_n of a leaf layer was calculated using multilayer model of photosynthesis (Terashima & Saeki, 1985; Evans, 1995) using absorbed light of a leaf layer and assuming a constant light saturated A_n (I_{inc} of 2200 μmol m^{-2} s^{-1}, CO_2 of 400 μmol mol^{-1}) across leaf depth. Model equations and more explanations of the calculations are given in Notes S3.

Estimating mesophyll conductance from carbon isotope discrimination measurements and leaf anatomical characteristics

Plants used for gas exchange and Chl fluorescence measurements and confocal microscopy were used. Some plants used in gas exchange measurement were measured for carbon isotope discrimination the next day, whereas those used in the microscopy were first measured for carbon isotope discrimination. Gas exchange measurements were conducted using a leaf gas exchange system, where simultaneously the CO_2 from reference and leaf cuvette air was sampled using two parallel cryogenic CO_2 trapping lines for carbon isotope discrimination analysis, following the procedure as described by Wassenaar *et al.* (2022). The youngest fully developed leaf was measured in four replicates by clamping the mid-position of the leaf using a leaf gas exchange system (LI-6800F; Li-Cor) with a 2 cm^2 aperture insert. The light intensity in the leaf cuvette was set at 2200 μmol m^{-2} s^{-1} (90% red, 10% blue). The leaf temperature was maintained at 25°C, and the CO_2 concentration was maintained at 420 ± 10 μmol mol^{-1}. Oxygen concentration was set at 2% to minimize the effect of fractionations due to photorespiration. Leaf-to-air vapor pressure deficit was between 1.0 and 1.6 kPa. After the steady states of A_n and g_s were achieved, air from the sample and reference lines of the gas exchange system were passed through parallel cryogenic trapping lines to sample CO_2 while gas exchange parameters were recorded for 15 min. The trapped CO_2 was then transferred into prevacuumed vials for isotopic composition analysis. The carbon isotope composition of the contents of the vials was analyzed using a dual-inlet isotope ratio mass spectrometer (SIRA series II, VG Isotech, modified by Provac Ltd, Crewe, UK).

The observed carbon isotope discrimination was calculated from the CO_2 concentrations and isotope ratios of sample and reference air used in the measurement. Mesophyll conductance based on carbon isotope discrimination measurement ($g_{m,13C}$) was calculated using equations as described by Evans & Von Caemmerer (2013) including the ternary corrections, assuming a fraction factor for Rubisco of 29‰, fractionation associated with respiration of −2.5‰, and fractionation associated with photorespiration of 12‰.

Mesophyll conductance calculated from leaf anatomical characteristics ($g_{m,ana}$) was used to assess the influence of leaf anatomical characteristics on variability of g_m among the species and in response to growth light intensity. The conductance of the intercellular airspace was based on mesophyll porosity assuming the effective path length of CO_2 in the intercellular airspace was a quarter of mesophyll thickness and a tortuosity of 1.57 m m^{-1} (Evans *et al.*, 2009; Niinemets *et al.*, 2009). The conductance of the liquid phase components was based on thicknesses of cell wall, cytosol and chloroplasts measured from electron microscopy images and assuming effective porosity of 0.20 for cell wall and permeability of 0.0035 m s^{-1} for plasma membrane and chloroplast envelop (Evans *et al.*, 2009; Evans, 2021). The conductance of the cell wall, plasma membrane and cytosol was scaled with $S_{m,a}$ and those of chloroplast envelop and stroma by S_c (Berghuijs

© 2024 The Author(s).
New Phytologist © 2024 New Phytologist Foundation.

14698137, 0, Downloaded from https://nph.onlinelibrary.wiley.com/doi/10.1111/nph.20136 by Wageningen University And Research Facilitair Bedrijf, Wiley Online Library on [21/10/2024]. See the Terms and Conditions (https://onlinelibrary.wiley.com/terms-and-conditions) on Wiley Online Library for rules of use; OA articles are governed by the applicable Creative Commons License

14698137, 0, Downloaded from https://nph.onlinelibrary.wiley.com/doi/10.1111/nph.20136 by Wageningen University And Research Facilitair Bedrijf, Wiley Online Library on [21/10/2024]. See the Terms and Conditions (https://onlinelibrary.wiley.com/terms-and-conditions) on Wiley Online Library for rules of use; OA articles are governed by the applicable Creative Commons License

et al., 2015). Model equations and parameters are given in Notes S4, Tables S1 and S2.

Relative limitation analysis

The relative limitations set by g_s (l_{gs}), g_m (l_{gm}) and maximum biochemical capacity V_{cmax} or J_{max} (l_{bio}) to changes in A_n were analyzed ($l_{gs} + l_{gm} + l_{bio} = 1$). $g_{m,cf}$ was used in the calculation. The l_{gs}, l_{gm} and l_{bio} were calculated using the relative limitation analysis method reported previously (Grassi & Magnani, 2005). Equations and more explanations of the calculations are given in Notes S2.

The relative limitation of g_m by the conductance of the intercellular airspace (l_{gas}) and the components of the liquid phase conductance (l_{liq}) such as cell wall, membranes, cytosol and stroma were calculated by dividing $g_{m,ana}$ by the respective conductance (Xiong, 2023). Equations and more explanations of the calculations are given in Notes S4.

Statistical analysis

Two-way analysis of variance (ANOVA) was carried out in R (v.4.2.2) to analyze the photosynthesis characteristics, the maximum photosynthetic capacity parameters, and anatomical parameters with species and growth light intensity as factors. Shapiro–Wilk test was used for normality and Levene's test of homogeneity to test for equal variance. Two-factor aligned rank transform ANOVA was used when assumptions of normality or equal variance were not met. Tukey's HSD *post hoc* test was performed when significant differences were found ($P < 0.05$).

Results

Photosynthesis rate and related physiological characteristics of the species

The photosynthesis rate and physiological traits were diverse among species in response to growth light intensity (Fig. 1). Notably, high-light-grown *H. incana*, *B. nigra* and *B. rapa* had similar net photosynthesis per leaf area ($A_{n,area}$) at the irradiance of 2200 μmol m^{-2} s^{-1} surpassing 40 μmol m^{-2} s^{-1}, exceeding that of *A. thaliana* (Fig. 1a). On dry mass basis ($A_{n,mass}$), *A. thaliana* and *B. rapa* had significantly higher $A_{n,mass}$ than *B. nigra* and *H. incana* under high light (Fig. 1b). Net photosynthesis on volume basis ($A_{n,volume}$) was similar among high-light plants (Fig. 1c). Under low light, *H. incana*, *B. nigra* had greater $A_{n,area}$, $A_{n,mass}$ and $A_{n,volume}$ than *A. thaliana* (Fig. 1a–c).

We further investigated important physiological traits influencing A_n and its response to changes in growth light intensity (Fig. 1d–f). A_n correlated positively and significantly with $g_{m,13C}$ (0.69 for low-light and 0.78 for high-light plants, Table S3) and g_s (0.75 for low light and 0.69 for high light plants, Table S3). Under high light, *B. rapa* exhibited the highest g_s and $g_{m,cf}$ (CO_2 of 400 μmol mol^{-1}, I_{inc} of 2200 μmol m^{-2} s^{-1}), followed by *H. incana*. *A. thaliana* and *B. nigra* had similar, significantly lower g_s values compared to *H. incana*, whereas $g_{m,cf}$ of *B. nigra* was intermediate between *H. incana* and *A. thaliana* (Figs 1d, 2a). Moreover, $g_{m,cf}$ and g_s were lower under low light than under high light for all species except *B. nigra*. Furthermore, there was a strong, significant linear relationship between $g_{m,cf}$ and $g_{m,13C}$ ($r^2 = 0.88$) and $g_{m,cf}$ and $g_{m,ana}$ ($r^2 = 0.79$), validating the trends in $g_{m,cf}$ (Fig. 2b,c).

We estimated V_{cmax}, J_{max} and T_p by fitting the A_n/C_i and A_n/I_{inc} curves to the biochemical model ($R^2 = 0.980$, Notes S2). The model predictions of the A_n/C_i and A_n/I_{inc} curves are shown in Fig. S2. The comparison of the V_{cmax} and J_{max} of the species are shown in Fig. 1(e,f) whereas the full set of parameters is given in Table S1. *Brassica nigra* had significantly higher V_{cmax}, J_{max} and T_p than *B. rapa* and *A. thaliana* under high light. *Brassica nigra* also had significantly higher V_{cmax} than *H. incana* but similar J_{max} under high light. Moreover, all species had significantly lower V_{cmax}, J_{max} and T_p under low light than under high light.

To assess the limitations of A_n by the maximum photosynthesis capacity, we calculated the C_i value at transition from Rubisco-limited to electron transport-limited rate and that from electron transport-limited rate to TPU-limited rate. The C_i values at ambient CO_2 of both high-light and low-light plants, except for *A. thaliana*, were within 50 μmol mol^{-1} of the C_i at the transition from Rubisco-limited to electron transport-limited rate (Table S4). In addition, in both high- and low-light conditions, photosynthesis was limited by V_{cmax}, except in low-light-grown *B. rapa* where it was limited by J_{max}. Moreover, the limitation by TPU occurred at $C_i \geq 650$ μmol mol^{-1} above which a decline in A_n was observed for *H. incana* and *B. rapa* (Tables S1, S4; Fig. S2).

Relative limitation by CO_2 conductance and biochemical capacity

Since the species exhibited contrasting maximum photosynthesis capacity and CO_2 conductance, we quantified their relative importance to photosynthesis rate. Fig. 3(a) shows the relative limitations to changes in A_n, differentiating them based on relative limitation by diffusional conductance (l_{gs}, l_{gm}) or by maximum photosynthesis capacity (l_{bio}).

In *A. thaliana*, l_{gm} and l_{bio} were similar under high-light condition and exceeded l_{gs}. For *B. rapa*, l_{bio} was the primary limitation under high- and low-light conditions. In *B. nigra*, all limitations were similar under high-light condition, whereas l_{bio} was the largest under low-light condition. With *H. incana*, l_{bio} was the main limitation to photosynthesis under high- and low-light conditions. In addition, l_{gs} and l_{gm} were similar under high light, whereas l_{gs} exceeded l_{gm} under low light in *H. incana*. Furthermore, the limitation by the total diffusional conductance ($l_{diff} = l_{gm} + l_{gs}$) was dominant in *A. thaliana* and *B. nigra* but not in *H. incana* and *B. rapa*, irrespective of growth light condition.

Growth under low light led to a higher l_{gm} in *B. rapa* and a lower one in *B. nigra* and *H. incana* (Fig. 3a). In addition, *B. nigra* had significantly higher l_{bio} under low light than under high light. Furthermore, *H. incana* had lower l_{diff}, whereas *B. rapa* had higher l_{diff} under low light (Fig. 3b).

© 2024 The Author(s).
New Phytologist © 2024 New Phytologist Foundation.

New Phytologist

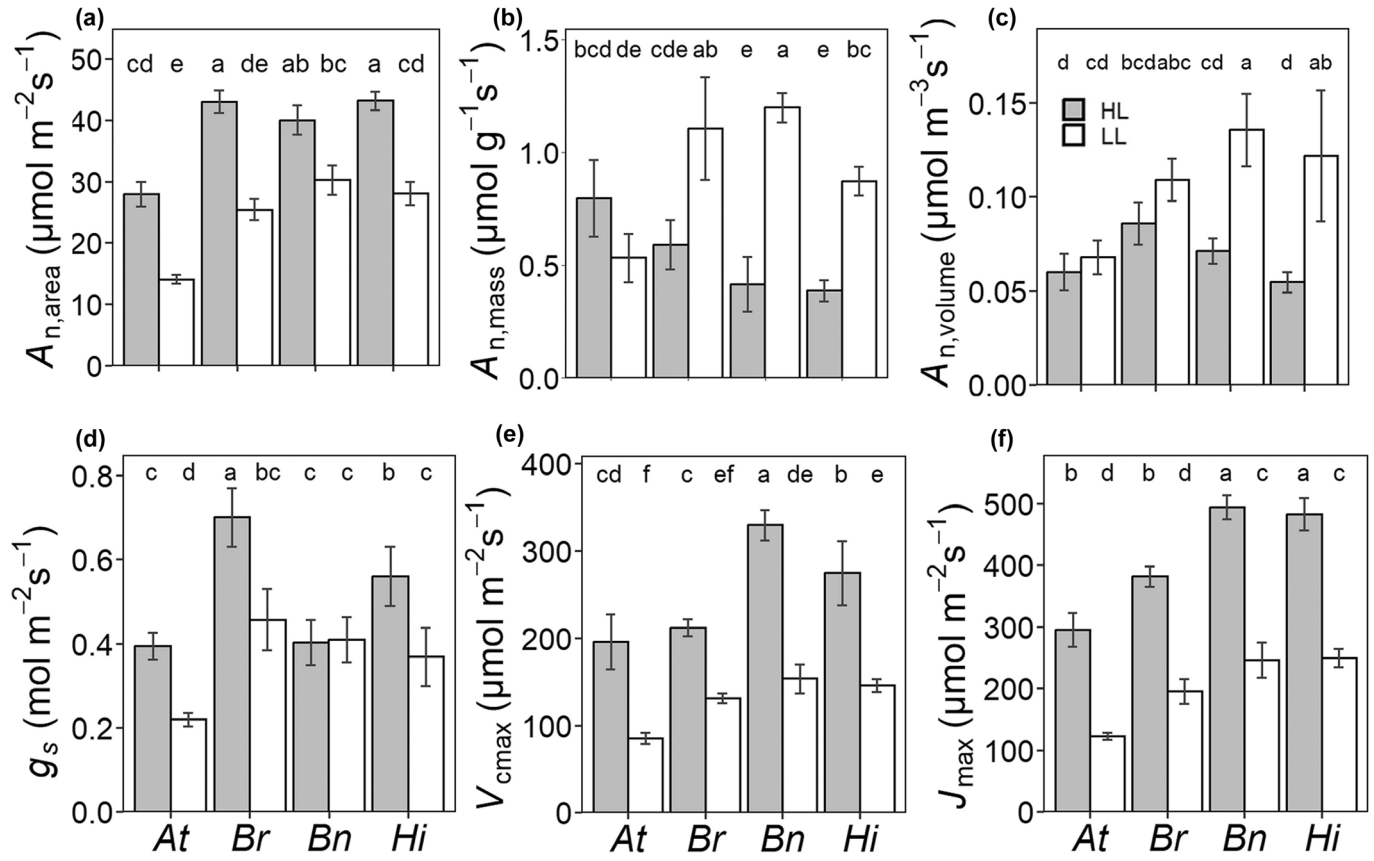


Fig. 1 Photosynthesis and related physiological characteristics. Net photosynthesis (A_n) per leaf area (panel a), per dry mass (panel b), per mesophyll volume (panel c), stomatal conductance to CO_2 (g_s, panel d), maximum carboxylation rate (V_{cmax}, panel e) and maximum rate of electron transport (J_{max}, panel f) for high-light (HL, gray bars) and low-light (LL, white bars) -grown plants of *Arabidopsis thaliana* (*At*), *Brassica rapa* (*Br*), *Brassica nigra* (*Bn*) and *Hirschfeldia incana* (*Hi*). A_n was measured at irradiance 2200 µmol m^{-2} s^{-1} and [CO_2] of 400 µmol mol^{-1}. Values are means ± SE (n = 4). Mean values not connected by similar letters were significantly different (Tukey's HSD test, $P < 0.05$).

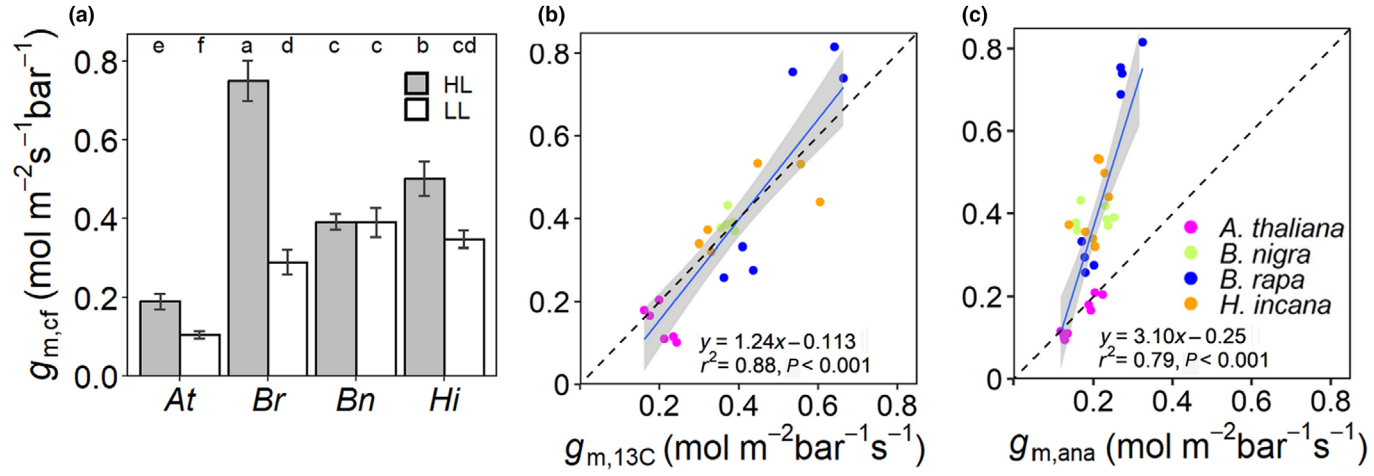


Fig. 2 Mesophyll conductance. Mesophyll conductance (g_m) estimated from combined gas exchange and Chl fluorescence ($g_{m,cf}$, panel a), panel b shows the relationship between $g_{m,cf}$ and g_m estimated from C-isotope discrimination measurement ($g_{m,13C}$), and panel c shows the relationship between $g_{m,cf}$ and g_m calculated from leaf anatomical properties ($g_{m,ana}$). g_m was calculated at [CO_2] of 400 µmol mol^{-1} and irradiance of 2200 µmol m^{-2} s^{-1} for high-light (HL) and low-light (LL) plants of *Arabidopsis thaliana* (*At*), *Brassica rapa* (*Br*), *Brassica.nigra* (*Bn*) and *Hirschfeldia incana* (*Hi*). Mean values (±SD) not connected by similar letters were significantly different (Tukey's HSD test, $P < 0.05$).

© 2024 The Author(s).
New Phytologist © 2024 New Phytologist Foundation.

14698137, 0, Downloaded from https://nph.onlinelibrary.wiley.com/doi/10.1111/nph.20136 by Wageningen University And Research Facilitair Bedrijf, Wiley Online Library on [21/10/2024]. See the Terms and Conditions (https://onlinelibrary.wiley.com/terms-and-conditions) on Wiley Online Library for rules of use; OA articles are governed by the applicable Creative Commons License

14698137, 0, Downloaded from https://nph.onlinelibrary.wiley.com/doi/10.1111/nph.20136 by Wageningen University And Research Facilitair Bedrijf, Wiley Online Library on [21/10/2024]. See the Terms and Conditions (https://onlinelibrary.wiley.com/terms-and-conditions) on Wiley Online Library for rules of use; OA articles are governed by the applicable Creative Commons License

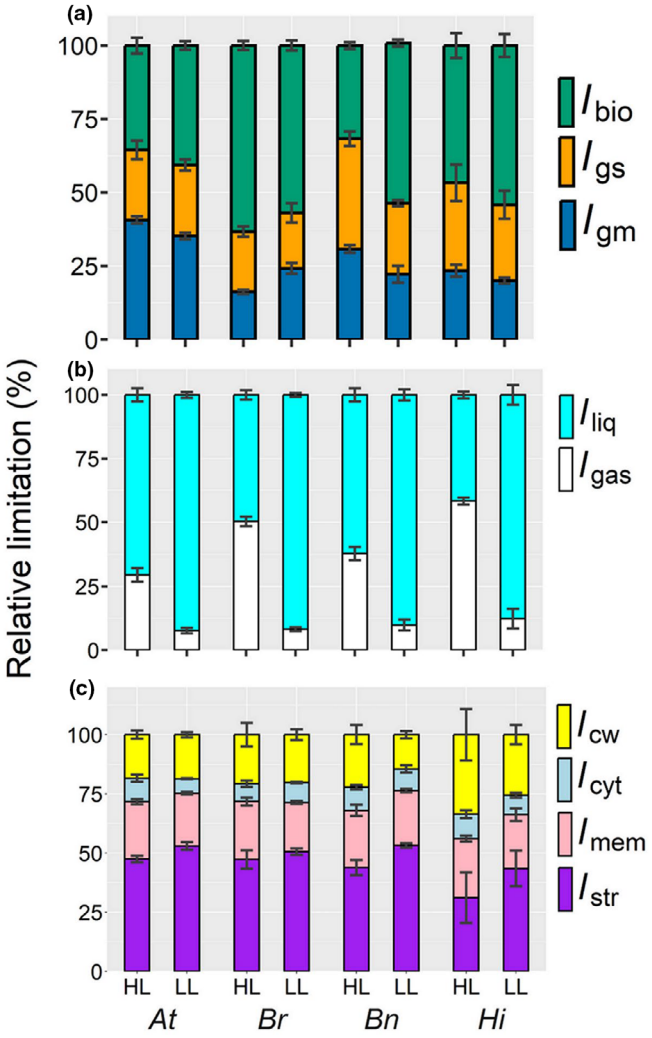


Fig. 3 Relative limitation to changes in photosynthesis and to mesophyll conductance. Panel a shows the relative limitation set by biochemical capacity (l_{bio}), by stomatal conductance (l_{gs}) and by mesophyll conductance (l_{gm}) to changes in photosynthesis. Panel b shows the relative limitation of mesophyll conductance by conductance of the liquid-phase diffusion (l_{liq}) and the gas-phase diffusion (l_{gas}). Panel c shows the relative limitation of mesophyll conductance by conductance of the cell wall (l_{cw}), cytosol (l_{cyt}), membranes (l_{mem}) and stroma (l_{str}). These relative limitations were calculated at $[CO_2]$ of 400 μmol mol^{-1} and irradiance of 2200 μmol m^{-2} s^{-1} for high-light (HL) and low-light (LL) plants. Mean ± SD.

Leaf traits contributing to variability in g_m and its acclimation responses

To identify leaf traits contributing to high g_m, a 1D mesophyll resistance model parametrized using anatomical measurements from leaf tissue images (Figs 3b,c, S3) was applied. Representative images of the leaf anatomy are shown in Figs 4 and S3. Fig. 5 shows selected leaf traits of the species in response to growth light intensity. Fig. 2(c) shows that $g_{m,ana}$ differed substantially from $g_{m,cf}$ suggesting that the variability in g_m could not be fully explained by the leaf anatomy. Notably, $g_{m,ana}$ and $g_{m,cf}$ were similar in *A. thaliana*. However, there was a significant positive correlation between $g_{m,ana}$ and $g_{m,cf}$ (Fig. 2c). In addition, the slope of the regression lines was significantly different from 1 (Fig. 2c). Therefore, we further analyzed the relative limitation by the components of the gas phase diffusion and liquid phase diffusion (Fig. 3b,c).

The relative limitation by the gas phase increased from *c.* 25% in *A. thaliana* to 58% in *H. incana* (Fig. 3b). The gas phase resistance was assumed to be influenced by the mesophyll porosity and thickness since tortuosity was assumed to be similar. Although $g_{m,cf}$ correlated weakly with mesophyll porosity, there was a significant positive correlation ($r > 0.60$) with $S_{m,a}$, S_c and $S_{m,v}$ both for high-light and low-light plants (Table S3). To this end, *H. incana* had significantly higher $S_{m,a}$ than *B. rapa* and *A. thaliana* under high light (Fig. 5c). The higher $g_{m,cf}$ of *B. nigra* and *B. rapa* than *A. thaliana* despite similar mesophyll thickness (Fig. 5a) suggests a contribution from leaf traits influencing the liquid phase diffusion.

The stroma and cell wall were the two most important limitations, accounting for more than 65% of the liquid-phase resistance, irrespective of growth light intensity (Fig. 3c). However, the thicknesses of the cell wall and stroma correlated weakly with $g_{m,cf}$ (Table S3). Notably, we assumed a constant effective porosity of the cell wall among the species and treatments. Furthermore, $S_{m,a}$ is a complex trait influenced by mesophyll thickness and $S_{m,v}$. There was 1.7-fold variation in mesophyll thickness (Fig. 5a) and 1.5-fold variation in $S_{m,v}$ (Fig. 5b) among high-light-grown species suggesting a strong contribution of the two in increasing $S_{m,a}$.

Brassica rapa and *Brassica nigra* had significantly greater $S_{m,v}$ than *A. thaliana* (Fig. 5b), despite having a similar mesophyll thickness (Fig. 5a). The leaf trait $S_{m,v}$ correlated positively with palisade cell density ($r = 0.65$, $P < 0.05$) and negatively with palisade cell diameter ($r = -0.72$, $P < 0.05$) (Table S3) for high-light plants. The higher palisade number density and smaller palisade diameter observed in *B. rapa* and *B. nigra* were consistent with the differences in $S_{m,v}$ (Fig. 5b). Furthermore, the higher g_m of *H. incana* than *A. thaliana* was contributed by a greater $S_{m,a}$ (Fig. 5c), which was enabled by a 1.7-fold higher mesophyll thickness (Fig. 5a) despite thicker cell wall in *H. incana* (Table S2) for similar palisade cell size and density (Fig. 5e,f).

Growth under low-light intensity increased the relative limitation by the liquid phase, which was brought about by 1.8- to 2.2-fold lower $S_{m,a}$ (Fig. 5b) under low light. In addition, there were 2.2- to 3.3-fold lower mesophyll thickness whereas $S_{m,v}$ remained similar, suggesting that mesophyll thickness had substantial contribution to the anatomically explained variability in g_m between high-light and low-light plants (Figs 2a, 5a,b).

Chlorophyll distribution, light absorption and photosynthesis capacity profiles of the species

Profiles of Chl content (representative images in Figs S4, S5), light absorption and photosynthesis are shown in Fig. 6. Relative Chl, derived from Chl fluorescence, increased up to a maximum at a relative depth of 82% for *B. nigra*, 79% for high-light-grown

© 2024 The Author(s).
New Phytologist © 2024 New Phytologist Foundation.

New Phytologist

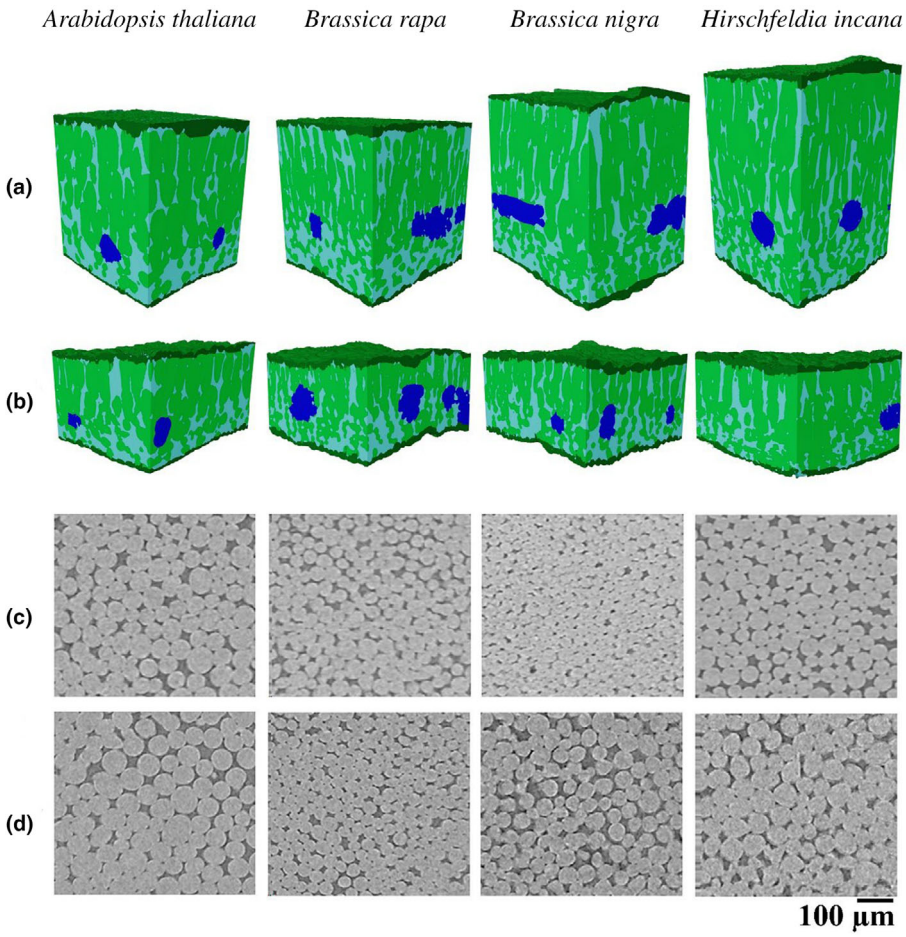


Fig. 4 The leaf anatomies of the plants grown under high light (a, c) and low light (b, d). Panels a and b show the 3D renderings of leaf tissue acquired from micro-CT scans consisting of epidermis (dark green), mesophyll (light green), intercellular airspace (cyan) and veins (blue). Panels c and d show paradermal sections made at 40% leaf thickness. Bar, 100 µm.

H. incana, 70% for *A. thaliana* and 50% for *B. rapa* (Fig. 6a). This differed significantly from the relative Chl profile in low-light-grown plants, where a maximum was reached earlier across the leaf depth (Fig. 6d).

The Chl profile was used to calculate the light absorption profile using Beer–Lambert's law and an apparent extinction coefficient. Both high- and low-light-grown plants show significant overlap in the absorption profile (Fig. 6b,e). The peak absorption occurred *c.* 13% of the relative leaf depth. Notably, *H. incana* had the lowest absorption at the depth for peak absorption (Fig. 6b,e). Furthermore, at the peak absorption, low-light plants absorbed more light than high-light plants (Fig. 6b,e). After the peak, the absorption declined more rapidly for low-light plants than for high-light plants. The photosynthesis capacity profile derived from the light absorption profile shows that photosynthesis was more uniform for high-light than low-light plants (Fig. 6c,f). *H. incana*, *B. nigra* and *B. rapa* had higher photosynthesis for the same relative depth than *A. thaliana* both under low- and high-light conditions (Fig. 6c,f).

Discussion

The exploration of natural variation in photosynthesis characteristics, coupled with in-depth species studies, emerges as a promising avenue for identifying traits that could enhance photosynthesis (Driever *et al.*, 2014; Gu *et al.*, 2014; Faralli & Lawson, 2020). In this study, we quantified the photosynthesis of three *Brassiceae* species – *H. incana*, *B. nigra* and *B. rapa* – grown under two contrasting light intensities and compared the outcome to measurements on the related model species *A. thaliana*. We also identified leaf traits contributing to high photosynthesis of the three *Brassiceae* species.

High photosynthesis rates in the *Brassiceae* species in relation to leaf traits

The wild mustard, *H. incana*, is well-adapted to high-light and dry environments (Taylor *et al.*, 2020; Garassino *et al.*, 2022), characterized by its thick leaves, which facilitate efficient thermoregulation and water storage (Terashima *et al.*, 2001, 2011; Oguchi *et al.*, 2003; Tholen *et al.*, 2012). The thick leaf of *H. incana* helped to increase leaf nitrogen content per area, which boosted the rate of electron transport and Rubisco carboxylation. These characteristics, commonly observed in plants grown under high light (Terashima *et al.*, 2001; Poorter *et al.*, 2019; Mathan *et al.*, 2021; Momayyezi *et al.*, 2022; Théroux-Rancourt *et al.*, 2023), led to a photosynthesis rate that is relatively less limited by the maximum photosynthesis capacity and more by CO_2 diffusion (Fig. 3a). The diffusion of CO_2 in the gas phase was more limiting for *H. incana* due to its thick leaf. However, the increase

© 2024 The Author(s).
New Phytologist © 2024 New Phytologist Foundation.

14698137, 0, Downloaded from https://nph.onlinelibrary.wiley.com/doi/10.1111/nph.20136 by Wageningen University And Research Facilitair Bedrijf, Wiley Online Library on [21/10/2024]. See the Terms and Conditions (https://onlinelibrary.wiley.com/terms-and-conditions) on Wiley Online Library for rules of use; OA articles are governed by the applicable Creative Commons License

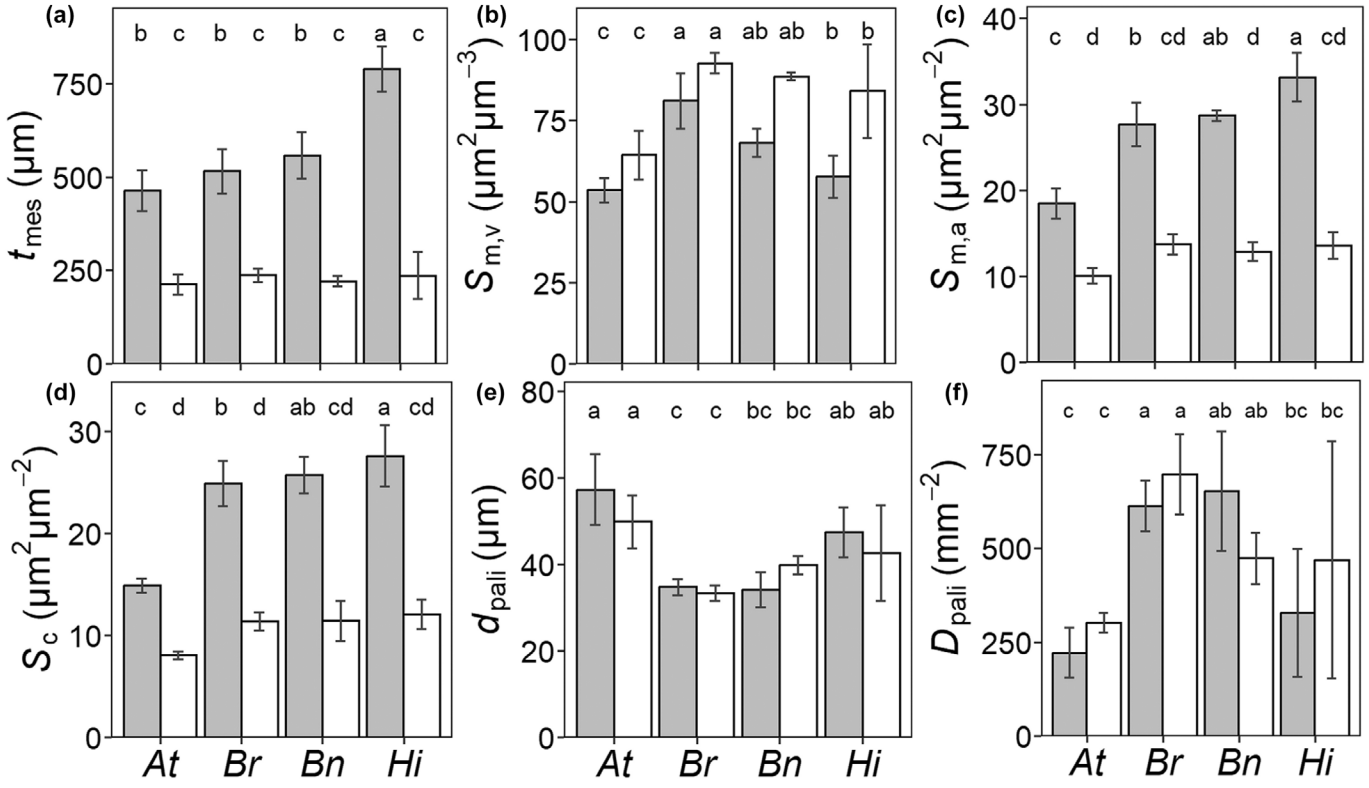


Fig. 5 Leaf anatomical characteristics. Mesophyll thickness (t_{mes}, panel a), exposed mesophyll surface (S_m) per mesophyll volume (S_m, v, panel b), S_m per leaf area ($S_{m,a}$, panel c), exposed chloroplast surface per leaf area (S_c) (panel d), palisade diameter (d_{pali}, panel e) and palisade number density (D_{pali}, panel f) for high-light (HL, gray bars) and low-light (LL, white bars) grown plants of *Arabidopsis thaliana* (*At*), *Brassica rapa* (*Br*), *Brassica nigra* (*Bn*) and *Hirschfeldia incana* (*Hi*). Means ± SE (n = 3). Mean values not connected by similar letters were significantly different (Tukey's HSD test, $P < 0.05$).

in $S_{m,a}$ due to a thicker leaf outweighed the increase in gas phase resistance, ultimately increasing $g_{m,cf}$ of *H. incana* over *A. thaliana*, which had a thinner leaf with similar $S_{m,v}$ (Figs 2, 5). However, its g_m fell within the higher range documented for C_3 plants (Niinemets *et al.*, 2009; Flexas *et al.*, 2012).

By contrast, the closely related crop species *B. nigra* achieved a similar high photosynthesis rate with a significantly thinner leaf and lower relative limitation set by V_{cmax} (Figs 1, 3, 4, 5). The higher V_{cmax} of *B. nigra* compared with *B. rapa* and *A. thaliana* could be explained by differences in Rubisco amount per leaf area, which can be inferred from leaf nitrogen content. In this regard, *B. nigra* exhibited higher leaf nitrogen content than *A. thaliana* when grown under high light (Table S1). Photosynthesis was relatively limited more by CO_2 diffusion since the low g_s in *B. nigra* reduced CO_2 supply and simultaneously decreased g_m despite having a thinner cell wall compared with *H. incana*. However, smaller and high-density palisade cells in *B. nigra* compared to *A. thaliana* boosted $S_{m,v}$ and increased $g_{m,cf}$ and $A_{n,area}$ in *B. nigra* for similar g_s.

Conversely, effective CO_2 transport in *B. rapa* increased photosynthesis in comparison with *A. thaliana*, facilitated by a high g_m and g_s, despite similar maximum photosynthesis capacity, leaf thickness and leaf dry mass per area. *Brassica rapa* had lower liquid phase diffusion resistance due to greater $S_{m,a}$ and S_c (Fig. 3; Table S2). At the anatomical level, the high density and small diameter of palisade cells in *B. rapa* contributed to a high $S_{m,v}$ (Fig. 5), which is shown to enhance CO_2 diffusion in the leaf (Tholen *et al.*, 2012; Ren *et al.*, 2019). Additionally, the high g_s might be achieved by small and high-density stomata (Franks *et al.*, 2009; Dow *et al.*, 2014), which is consistent with *B. rapa*'s stomatal characteristics (Table S2).

A high photosynthesis rate under high-light intensity requires not only high CO_2 diffusion and biochemical capacity but also efficient light use, which is influenced by mesophyll structure, for a greater rate of electron transport under the constraints of photodamage (von Caemmerer & Farquhar, 1981; Cui *et al.*, 1991; Vogelmann & Martin, 1993; Terashima *et al.*, 2011; von Caemmerer, 2013; Ichiro *et al.*, 2016). The gradual increase in Chl content along the leaf depth in the species, a pattern consistent with a previous report for many C_3 plants (Borsuk & Brodersen, 2019), will avoid exposure to excess light (Slattery *et al.*, 2016; Borsuk & Brodersen, 2019). Despite the relatively thick leaves of *H. incana*, Chl was distributed relatively similarly in comparison with thinner leaves. This resulted in a similar relative light absorption profile, but its thicker leaf can potentially accommodate more chloroplasts and such conditions support a greater electron transport rate, as observed in *H. incana* (Table S4). Consequently, *H. incana* had higher photosynthesis capacity for similar relative depth, which was also more uniformly distributed (Fig. 6c,f).

In summary, our findings indicate that enhancing photosynthesis can indeed be achieved by strategically manipulating leaf

© 2024 The Author(s).
New Phytologist © 2024 New Phytologist Foundation.

14698137, 0, Downloaded from https://nph.onlinelibrary.wiley.com/doi/10.1111/nph.20136 by Wageningen University And Research Facilitair Bedrijf, Wiley Online Library on [21/10/2024]. See the Terms and Conditions (https://onlinelibrary.wiley.com/terms-and-conditions) on Wiley Online Library for rules of use; OA articles are governed by the applicable Creative Commons License

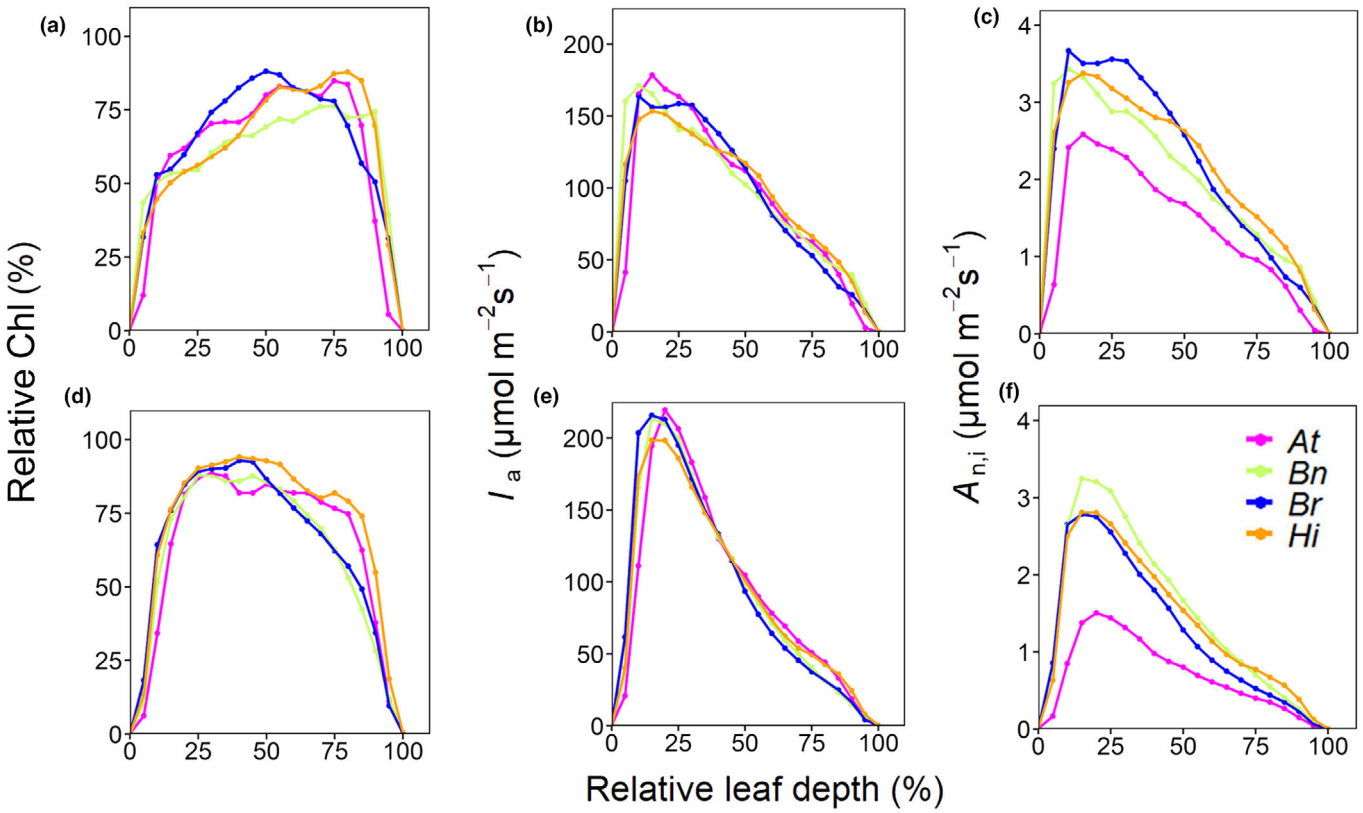


Fig. 6 Profiles of the relative Chl content, absorbed light and net photosynthesis. Shown are the profiles of relative Chl (a, d), absorbed light (I_a, b, e) and net photosynthesis of a leaf layer ($A_{n,i}$, c,f) of *Arabidopsis thaliana* (*At*), *Brassica nigra* (*Bn*), *Brassica rapa* (*Br*) and *Hirschfeldia incana* (*Hi*), grown under high light (HL, a–c) and low light (LL, d–f). Data points are mean values sampled at every 5% leaf depth per species under HL or LL condition. Error bars were removed for clarity here but are shown in Figs S4 and S5.

anatomy to increase g_m and g_s (Adachi *et al.*, 2013; Lehmeier *et al.*, 2017; Lundgren *et al.*, 2019; Ren *et al.*, 2019; Lundgren & Fleming, 2020; Mathan *et al.*, 2021). Addressing biochemical rate limitations by selecting plants with thicker leaves or mesophyll structure with a high surface to volume ratio, while ensuring efficient light distribution and CO_2 diffusion can be effective, yet recognizing the importance of a speedy canopy closure for an improved crop light interception (Yin & Struik, 2015; Mathan *et al.*, 2021; Zeng *et al.*, 2022).

Impact of low light on photosynthesis of the *Brassiceae* species

The lower values of $A_{n,area}$ and CO_2 conductance in many of the species when growing under low light than when grown under high light was consistent with previous reports (Oguchi *et al.*, 2003; Anderson *et al.*, 2021; Zeng *et al.*, 2022; Théroux-Rancourt *et al.*, 2023). Acclimation to low light involved a major change in mesophyll thickness, maximum photosynthesis capacity and CO_2 conductance rather than Chl content and light absorbance (Table S1). The change in mesophyll thickness was because of fewer layers of palisade cells (Figs 4, S3), which suggests acclimation to low light through lower cell division (Tosens *et al.*, 2012; Lehmeier *et al.*, 2017). The smaller mesophyll thickness led to lower nitrogen content and maximum photosynthetic capacity, thereby increasing the relative limitation to changes in photosynthesis rate set by maximum photosynthesis capacity (Fig. 3a). Furthermore, *H. incana* and *B. nigra* exhibited differential construction strategies in responses to low light than *B. rapa* and *A. thaliana* (Fig. 1b,c). The higher $A_{n,mass}$ and $A_{n,volume}$ of *H. incana* under low light than high light suggests a higher allocation of leaf mass to support structures, which is supported by thicker cell wall under high light (Fig. 1b; Table S2). The contrasting responses could be explained by genetic relationships: *A. thaliana* and *B. rapa* are genetically close to each other than to *B. nigra* and *H. incana*, which in turn are closer to each other (Arias & Pires, 2012; Garassino *et al.*, 2022). Moreover, the maximum relative Chl content was shifted to the adaxial leaf side that allowed for better use of the low-light intensity (Fig. 6e,f).

Limitations and future perspectives

The exploration of high photosynthesis rate at high-light intensity in the species involved the assessment of many plants, limiting the ability to measure all leaf traits on a per plant basis. The similarity in mesophyll thickness of the leaves from different sets of plants (Fig. S6) reflects the success of efforts to standardize growth conditions and sampling. However, the possibility that

© 2024 The Author(s).
New Phytologist © 2024 New Phytologist Foundation.

14698137, 0, Downloaded from https://nph.onlinelibrary.wiley.com/doi/10.1111/nph.20136 by Wageningen University And Research Facilitair Bedrijf, Wiley Online Library on [21/10/2024]. See the Terms and Conditions (https://onlinelibrary.wiley.com/terms-and-conditions) on Wiley Online Library for rules of use; OA articles are governed by the applicable Creative Commons License

14698137, 0, Downloaded from https://nph.onlinelibrary.wiley.com/doi/10.1111/nph.20136 by Wageningen University And Research Facilitair Bedrijf, Wiley Online Library on [21/10/2024]. See the Terms and Conditions (https://onlinelibrary.wiley.com/terms-and-conditions) on Wiley Online Library for rules of use; OA articles are governed by the applicable Creative Commons License

inherent variations among individual plants in the different experiments may have contributed to the observed differences could not be excluded. Furthermore, $g_{m,ana}$ and the predicted profile of photosynthesis across leaf depth could be more accurately investigated using a 3D reaction–diffusion models for CO_2 (Berghuijs *et al.*, 2015; Ho *et al.*, 2016; Retta *et al.*, 2023). S_c was estimated from 2D images, which could lead to a bias (Harwood *et al.*, 2020). Moreover, the observed differences in maximum photosynthetic capacity among the three species warrant a future investigation into the enzymatic properties of Rubisco and electron transport proteins. Finally, the genetic causes of the observed phenotypes should be explored to find more clues to enhance photosynthesis.

Conclusion

Our findings for photosynthesis rates of *H. incana*, *B. nigra* and *B. rapa* and the model plant *A. thaliana* show that achieving a high photosynthesis rate under high-light conditions involved a combination of species-specific anatomical, photosynthetic capacity and physiological acclimations. The similar photosynthesis rates among *H. incana*, *B. nigra* and *B. nigra* despite their distinct traits suggest a convergence of physiological and anatomical acclimations that promote efficient CO_2 assimilation. Overall, the leaf anatomy enabled high photosynthesis rate by facilitating rapid CO_2 diffusion, enabling efficient light use and providing ample volume for high photosynthetic capacity.

Acknowledgements

We thank Francesco Garassino and Ludovico Caracciolo for their invaluable assistance in conducting the gas exchange measurements and stomata analysis, Maarten Wassenaar, Peter van der Putten and Leon Mossink for their technical assistance with leaf absorbance, CO_2 cryotrapping and gas exchange measurements, and Arjen van de Peppel for help with Chl content analysis. We also express our appreciation to Jeremy Harbinson for discussions that enriched our research. We acknowledge the assistance of Prof. Johan Billen and An Vandoren from KU Leuven, and Jose van de Belt from Wageningen University and Research, during the light and electron microscopy experiment. KU Leuven authors acknowledge the financial support of the Research Foundation – Flanders (FWO Vlaanderen, SBO project FoodPhase, grant no. S003421N), and KU Leuven (project C14/22/076). X-ray computed tomography was performed at the XCT Core Facility of KU Leuven.

Competing interests

None declared.

Author contributions

PCS, XY and SMD conceived and designed the research; MAR and LVD performed the experiments and analyzed the data; MAR wrote the manuscript with contributions from LVD; PCS, XY, SMD, NCAR, PV, BMN and LVD reviewed the manuscript. All authors read and approved the final version of the manuscript.

ORCID

Steven M. Driever https://orcid.org/0000-0003-4144-6028
Bart M. Nicolaï https://orcid.org/0000-0001-5267-1920
Moges A. Retta https://orcid.org/0000-0002-4835-7274
Norbert C. A. de Ruijter https://orcid.org/0000-0003-3746-9403
Paul C. Struik https://orcid.org/0000-0003-2196-547X
Leen Van Doorselaer https://orcid.org/0000-0002-0811-1616
Pieter Verboven https://orcid.org/0000-0001-9542-8285
Xinyou Yin https://orcid.org/0000-0001-8273-8022

Data availability

All the raw data, microscopy images of leaf anatomy, Chl and light profile and gas exchange, supporting the results are available on Zenodo (https://zenodo.org/records/10057959). X-ray micro-CT images are available on: http://www.x-plant.org/leaves/Leaves.

References

Adachi S, Nakae T, Uchida M, Soda K, Takai T, Oi T, Yamamoto T, Ookawa T, Miyake H, Yano M *et al.* 2013. The mesophyll anatomy enhancing CO_2 diffusion is a key trait for improving rice photosynthesis. *Journal of Experimental Botany* **64**: 1061–1072.

Anderson CM, Mattoon EM, Zhang N, Becker E, McHargue W, Yang J, Patel D, Dautermann O, McAdam SAM, Tarin T *et al.* 2021. High light and temperature reduce photosynthetic efficiency through different mechanisms in the C4 model Setaria viridis. *Communications Biology* **4**: 1092.

Arias T, Pires JC. 2012. A fully resolved chloroplast phylogeny of the brassica crops and wild relatives (Brassicaceae: Brassiceae): novel clades and potential taxonomic implications. *Taxon* **61**: 980–988.

Berghuijs HNC, Yin X, Tri Ho Q, van der Putten PELL, Verboven P, Retta MA, Nicolaï BM, Struik PC. 2015. Modelling the relationship between CO_2 assimilation and leaf anatomical properties in tomato leaves. *Plant Science* **238**: 297–311.

Boardman NK. 1977. Comparative photosynthesis of sun and shade plants. *Annual Review of Plant Physiology* **28**: 355–377.

Borsuk AM, Brodersen CR. 2019. The spatial distribution of chlorophyll in leaves. *Plant Physiology* **180**: 1406–1417.

von Caemmerer S. 2013. Steady-state models of photosynthesis. *Plant, Cell & Environment* **36**: 1617–1630.

von Caemmerer S, Farquhar GD. 1981. Some relationships between the biochemistry of photosynthesis and the gas exchange of leaves. *Planta* **153**: 376–387.

Cui M, Vogelmann TC, Smith WK. 1991. Chlorophyll and light gradients in sun and shade leaves of Spinacia oleracea. *Plant, Cell & Environment* **14**: 493–500.

Dow GJ, Bergmann DC, Berry JA. 2014. An integrated model of stomatal development and leaf physiology. *New Phytologist* **201**: 1218–1226.

Driever SM, Lawson T, Andralojc PJ, Raines CA, Parry MAJ. 2014. Natural variation in photosynthetic capacity, growth, and yield in 64 field-grown wheat genotypes. *Journal of Experimental Botany* **65**: 4959–4973.

© 2024 The Author(s).
New Phytologist © 2024 New Phytologist Foundation.

Earles JM, Buckley TN, Brodersen CR, Busch FA, Cano FJ, Choat B, Evans JR, Farquhar GD, Harwood R, Huynh M *et al.* 2019. Embracing 3D complexity in leaf carbon–water exchange. *Trends in Plant Science* **24**: 15–24.

Earles JM, Theroux-Rancourt G, Roddy AB, Gilbert ME, McElrone AJ, Brodersen CR. 2018. Beyond porosity: 3D leaf intercellular airspace traits thatimpact mesophyll conductance. *Plant Physiology* **178**: 148–162.

Evans J. 1995. Carbon fixation profiles do reflect light absorption profiles in leaves. *Functional Plant Biology* **22**: 865.

Evans JR. 2013. Improving photosynthesis. *Plant Physiology* **162**: 1780–1793.

Evans JR. 2021. Mesophyll conductance: walls, membranes and spatial complexity. *New Phytologist* **229**: 1864–1876.

Evans JR, Kaldenhoff R, Genty B, Terashima I. 2009. Resistances along the CO_2 diffusion pathway inside leaves. *Journal of Experimental Botany* **60**: 2235–2248.

Evans JR, Von Caemmerer S. 2013. Temperature response of carbon isotope discrimination and mesophyll conductance in tobacco. *Plant, Cell & Environment* **36**: 745–756.

Faralli M, Lawson T. 2020. Natural genetic variation in photosynthesis: an untapped resource to increase crop yield potential? *The Plant Journal* **101**: 518–528.

Farquhar GD, von Caemmerer S, Berry JA. 1980. A biochemical model of photosynthetic CO_2 assimilation in leaves of C3 species. *Planta* **149**: 78–90.

Flexas J, Barbour MM, Brendel O, Cabrera HM, Carriquí M, Díaz-Espejo A, Douthe C, Dreyer E, Ferrio JP, Gago J *et al.* 2012. Mesophyll diffusion conductance to CO2: an unappreciated central player in photosynthesis. *Plant Science* **193–194**: 70–84.

Franks PJ, Drake PL, Beerling DJ. 2009. Plasticity in maximum stomatal conductance constrained by negative correlation between stomatal size and density: an analysis using *Eucalyptus globulus*. *Plant, Cell & Environment* **32**: 1737–1748.

Garassino F, Wijfjes RY, Boesten R, Reyes Marquez F, Becker FFM, Clapero V, van den Hatert I, Holmer R, Schranz ME, Harbinson J *et al.* 2022. The genome sequence of *Hirschfeldia incana*, a new Brassicaceae model to improve photosynthetic light-use efficiency. *The Plant Journal* **112**: 298–1315.

Genty B, Briantais J-M, Baker NR. 1989. The relationship between the quantum yield of photosynthetic electron transport and quenching of chlorophyll fluorescence. *Biochimica et Biophysica Acta (BBA) – General Subjects* **990**: 87–92.

Grassi G, Magnani F. 2005. Stomatal, mesophyll conductance and biochemical limitations to photosynthesis as affected by drought and leaf ontogeny in ash and oak trees. *Plant, Cell & Environment* **28**: 834–849.

Gu J, Yin X, Stomph T-J, Struik PC. 2014. Can exploiting natural genetic variation in leaf photosynthesis contribute to increasing rice productivity? A simulation analysis: Photosynthetic variation and rice productivity. *Plant, Cell & Environment* **37**: 22–34.

Harwood R, Goodman E, Gudmundsdottir M, Huynh M, Musulin Q, Song M, Barbour MM. 2020. Cell and chloroplast anatomical features are poorly estimated from 2D cross-sections. *New Phytologist* **225**: 2567–2578.

Ho QT, Berghuijs HNC, Watté R, Verboven P, Herremans E, Yin X, Retta MA, Aernouts B, Saeys W, Helfen L *et al.* 2016. Three-dimensional microscale modelling of CO_2 transport and light propagation in tomato leaves enlightens photosynthesis. *Plant, Cell & Environment* **39**: 50–61.

Hoshino R, Yoshida Y, Tsukaya H. 2019. Multiple steps of leaf thickening during sun-leaf formation in Arabidopsis. *The Plant Journal* **100**: 738–753.

Ichiro T, Hiroki O, Takashi F, Riichi O. 2016. Light environment within a leaf. II. Progress in the past one-third century. *Journal of Plant Research* **129**: 353–363.

Knauer J, Cuntz M, Evans JR, Niinemets Ü, Tosens T, Veromann-Jürgenson L, Werner C, Zaehle S. 2022. Contrasting anatomical and biochemical controls on mesophyll conductance across plant functional types. *New Phytologist* **236**: 357–368.

Lehmeier C, Pajor R, Lundgren MR, Mathers A, Sloan J, Bauch M, Mitchell A, Bellasio C, Green A, Bouyer D *et al.* 2017. Cell density and airspace patterning in the leaf can be manipulated to increase leaf photosynthetic capacity. *The Plant Journal* **92**: 981–994.

Loriaux SD, Avenson TJ, Welles JM, Mcdermitt DK, Eckles RD, Reinsche B, Genty B. 2013. Closing in on maximum yield of chlorophyll fluorescence using a single multiphase flash of sub-saturating intensity. *Plant, Cell & Environment* **36**: 1755–1770.

Lundgren MR, Fleming AJ. 2020. Cellular perspectives for improving mesophyll conductance. *The Plant Journal* **101**: 845–857.

Lundgren MR, Mathers A, Baillie AL, Dunn J, Wilson MJ, Hunt L, Pajor R, Fradera-Soler M, Rolfe S, Osborne CP *et al.* 2019. Mesophyll porosity is modulated by the presence of functional stomata. *Nature Communications* **10**: 2825.

Mathan J, Singh A, Jathar V, Ranjan A. 2021. High photosynthesis rate in two wild rice species is driven by leaf anatomy mediating high Rubisco activity and electron transport rate. *Journal of Experimental Botany* **72**: 7119–7135.

Mathers AW, Hepworth C, Baillie AL, Sloan J, Jones H, Lundgren M, Fleming AJ, Mooney SJ, Sturrock CJ. 2018. Investigating the microstructure of plant leaves in 3D with lab-based X-ray computed tomography. *Plant Methods* **14**: 99.

Momayyezi M, Borsuk AM, Brodersen CR, Gilbert ME, Théroux-Rancourt G, Kluepfel DA, McElrone AJ. 2022. Desiccation of the leaf mesophyll and its implications for CO_2 diffusion and light processing. *Plant, Cell & Environment* **45**: 1362–1381.

Niinemets U, Wright IJ, Evans JR. 2009. Leaf mesophyll diffusion conductance in 35 Australian sclerophylls covering a broad range of foliage structural and physiological variation. *Journal of Experimental Botany* **60**: 2433–2449.

Oguchi R, Hikosaka K, Hirose T. 2003. Does the photosynthetic light-acclimation need change in leaf anatomy? *Plant, Cell & Environment* **26**: 505–512.

Ort DR, Merchant SS, Alric J, Barkan A, Blankenship RE, Bock R, Croce R, Hanson MR, Hibberd JM, Long SP *et al.* 2015. Redesigning photosynthesis to sustainably meet global food and bioenergy demand. *Proceedings of the National Academy of Sciences, USA* **112**: 201424031.

Poorter H, Niinemets Ü, Ntagkas N, Siebenkäs A, Mäenpää M, Matsubara S, Pons TL. 2019. A meta-analysis of plant responses to light intensity for 70 traits ranging from molecules to whole plant performance. *New Phytologist* **223**: 1073–1105.

Ren T, Weraduwage SM, Sharkey TD. 2019. Prospects for enhancing leaf photosynthetic capacity by manipulating mesophyll cell morphology. *Journal of Experimental Botany* **70**: 1153–1165.

Retta MA, Yin X, Ho QT, Watté R, Berghuijs HNC, Verboven P, Saeys W, Cano FJ, Ghannoum O, Struik PC *et al.* 2023. The role of chloroplast movement in C4 photosynthesis: a theoretical analysis using a three-dimensional reaction–diffusion model for maize. *Journal of Experimental Botany* **74**: 4125–4142.

Schlüter U, Bouvier JW, Guerreiro R, Malisic M, Kontny C, Westhoff P, Stich B, Weber APM. 2023. Brassicaceae display variation in efficiency of photorespiratory carbon-recapturing mechanisms. *Journal of Experimental Botany* **74**: 6631–6649.

Simkin AJ, López-Calcagno PE, Raines CA. 2019. Feeding the world: improving photosynthetic efficiency for sustainable crop production. *Journal of Experimental Botany* **70**: 1119–1140.

Slattery RA, Grennan AK, Sivaguru M, Sozzani R, Ort DR. 2016. Light sheet microscopy reveals more gradual light attenuation in light-green versus dark-green soybean leaves. *Journal of Experimental Botany* **67**: 4697–4709.

Stringer C, Wang T, Michaelos M, Pachitariu M. 2021. Cellpose: a generalist algorithm for cellular segmentation. *Nature Methods* **18**: 100–106.

Taylor G, Garassino F, Aarts MGM, Harbinson J. 2022. Improving C3 photosynthesis by exploiting natural genetic variation: *Hirschfeldia incana* as a model species. *Food and Energy Security* **12**: e420.

Taylor SH, Orr DJ, Carmo-Silva E, Long SP. 2020. During photosynthetic induction, biochemical and stomatal limitations differ between *Brassica* crops. *Plant, Cell & Environment* **43**: 2623–2636.

Terashima I, Hanba YT, Tholen D, Niinemets Ü. 2011. Leaf functional anatomy in relation to photosynthesis. *Plant Physiology* **155**: 108–116.

Terashima I, Miyazawa S-I, Hanba YT. 2001. Why are sun leaves thicker than shade leaves? – consideration based on analyses of CO_2 diffusion in the leaf. *Journal of Plant Research* **114**: 93–105.

Terashima I, Saeki T. 1985. A new model for leaf photosynthesis incorporating the gradients of light environment and of photosynthetic properties of chloroplasts within a leaf. *Annals of Botany* **56**: 489–499.

© 2024 The Author(s).
New Phytologist © 2024 New Phytologist Foundation.

14698137, 0, Downloaded from https://nph.onlinelibrary.wiley.com/doi/10.1111/nph.20136 by Wageningen University And Research Facilitair Bedrijf, Wiley Online Library on [21/10/2024]. See the Terms and Conditions (https://onlinelibrary.wiley.com/terms-and-conditions) on Wiley Online Library for rules of use; OA articles are governed by the applicable Creative Commons License

Théroux-Rancourt G, Herrera JC, Voggeneder K, De Berardinis F, Luijken N, Nocker L, Savi T, Scheffknecht S, Schneck M, Tholen D. 2023. Analyzing anatomy over three dimensions unpacks the differences in mesophyll diffusive area between sun and shade *Vitis vinifera* leaves. *AoB Plants* **15**: plad001.

Théroux-Rancourt G, Jenkins MR, Brodersen CR, McElrone A, Forrestel EJ, Earles JM. 2020. Digitally deconstructing leaves in 3D using X-ray microcomputed tomography and machine learning. *Applications in Plant Sciences* **8**: e11380.

Théroux-Rancourt G, Roddy AB, Earles JM, Gilbert ME, Zwieniecki MA, Boyce CK, Tholen D, McElrone AJ, Simonin KA, Brodersen CR. 2021. Maximum CO_2 diffusion inside leaves is limited by the scaling of cell size and genome size. *Proceedings of the Royal Society B: Biological Sciences* **288**: 20203145.

Tholen D, Boom C, Zhu X-G. 2012. Opinion: prospects for improving photosynthesis by altering leaf anatomy. *Plant Science* **197**: 92–101.

Tosens T, Niinemets Ü, Vislap V, Eichelmann H, Castro DP. 2012. Developmental changes in mesophyll diffusion conductance and photosynthetic capacity under different light and water availabilities in Populus tremula: how structure constrains function. *Plant, Cell & Environment* **35**: 839–856.

Vogelmann TC, Evans JR. 2002. Profiles of light absorption and chlorophyll within spinach leaves from chlorophyll fluorescence. *Plant, Cell & Environment* **25**: 1313–1323.

Vogelmann TC, Martin G. 1993. The functional significance of palisade tissue: penetration of directional versus diffuse light. *Plant, Cell & Environment* **16**: 65–72.

Wassenaar MLJ, van Ieperen W, Driever SM. 2022. Low red to far-red ratio increases resistance to CO_2 diffusion and reduces photosynthetic efficiency in low light grown tomato plants. *Environmental and Experimental Botany* **200**: 104918.

Wellburn AR. 1994. The spectral determination of chlorophylls a and b, as well as total carotenoids, using various solvents with spectrophotometers of different resolution. *Journal of Plant Physiology* **144**: 307–313.

Xiong D. 2023. Leaf anatomy does not explain the large variability of mesophyll conductance across C3 crop species. *The Plant Journal* **113**: 1035–1048.

Yamori W, Kondo E, Sugiura D, Terashima I, Suzuki Y, Makino A. 2016. Enhanced leaf photosynthesis as a target to increase grain yield: insights from transgenic rice lines with variable Rieske FeS protein content in the cytochrome b6f complex. *Plant, Cell & Environment* **39**: 80–87.

Yin X, Amthor JS. 2024. Estimating leaf day respiration from conventional gas exchange measurements. *New Phytologist* **241**: 52–58.

Yin X, Busch FA, Struik PC, Sharkey TD. 2021. Evolution of a biochemical model of steady-state photosynthesis. *Plant, Cell & Environment* **44**: 2811–2837.

Yin X, Struik PC. 2015. Constraints to the potential efficiency of converting solar radiation into phytoenergy in annual crops: from leaf biochemistry to canopy physiology and crop ecology. *Journal of Experimental Botany* **66**: erv371.

Yin X, Struik PC, Romero P, Harbinson J, Evers JB, Van Der Putten PEL, Vos J. 2009. Using combined measurements of gas exchange and chlorophyll fluorescence to estimate parameters of a biochemical C3 photosynthesis model: a critical appraisal and a new integrated approach applied to leaves in a wheat (*Triticum aestivum*) canopy. *Plant, Cell & Environment* **32**: 448–464.

Zeng F, Zhu L, Wang G, Liang Y, Ma D, Wang J. 2022. Higher CO_2 assimilation in selected rice recombinant Inbred lines is driven by higher CO_2 diffusion and light use efficiency related to leaf anatomy and mesophyll cell density. *Frontiers in Plant Science* **13**: 915050.

Zhu X-G, Long SP, Ort DR. 2010. Improving photosynthetic efficiency for greater yield. *Annual Review of Plant Biology* **61**: 235–261.

Supporting Information

Additional Supporting Information may be found online in the Supporting Information section at the end of the article.

Fig. S1 Segmentation workflow of leaf tissue micro-CT images.

Fig. S2 Response of net photosynthesis to [CO_2] and irradiance.

Fig. S3 Representative images of leaf structure.

Fig. S4 Representative images of relative Chl profile of high-light-grown species.

Fig. S5 Representative images of relative Chl profile of low-light-grown species.

Fig. S6 Comparison of mesophyll thickness across the used imaging methods.

Notes S1 X-ray micro-CT image processing steps and calculations of leaf anatomical parameters.

Notes S2 Biochemical model of C_3 photosynthesis.

Notes S3 Multilayer leaf model.

Notes S4 A 1-D mesophyll conductance model.

Table S1 Photosynthesis and related physiological characteristics of the species.

Table S2 Leaf anatomical characteristics of the species.

Table S3 Pair-wise Pearson's correlation coefficients for correlations among the leaf photosynthesis and physiological traits.

Table S4 Intercellular CO_2 concentrations and electron transport rate.

Please note: Wiley is not responsible for the content or functionality of any Supporting Information supplied by the authors. Any queries (other than missing material) should be directed to the *New Phytologist* Central Office.

© 2024 The Author(s).
New Phytologist © 2024 New Phytologist Foundation.

14698137, 0, Downloaded from https://nph.onlinelibrary.wiley.com/doi/10.1111/nph.20136 by Wageningen University And Research Facilitair Bedrijf, Wiley Online Library on [21/10/2024]. See the Terms and Conditions (https://onlinelibrary.wiley.com/terms-and-conditions) on Wiley Online Library for rules of use; OA articles are governed by the applicable Creative Commons License